Melting of crystals of polarization vortices and chiral phase transitions in oxide superlattices

Fernando Gómez-Ortiz[1], Pablo García-Fernández,[1] Juan M. López[2] and Javier Junquera[1,*]

[1]*Departamento de Ciencias de la Tierra y Física de la Materia Condensada, Universidad de Cantabria,*
Cantabria Campus Internacional, Avenida de los Castros s/n, 39005 Santander, Spain

[2]*Instituto de Física de Cantabria (IFCA), CSIC-Universidad de Cantabria, 39005 Santander, Spain*

We study the equilibrium arrangements of polarization vortices in $(PbTiO_3)_n/(SrTiO_3)_n$ superlattices by means of second-principles simulations. We find that, at low temperatures, polarization vortices organize in a regular arrangement in which clockwise and counterclockwise vortices alternate positions, leading to a crystal-like structure with well-defined handedness. This chiral crystal melts at a critical temperature T_M into a chiral liquid where long-range order is lost but handedness is preserved. At even higher temperatures T_C, a second phase transition occurs at which the chiral liquid of polarization vortices loses its handedness. Both phase transitions can be readily identified by the adequate choices of order parameters.

Over the past few years, the existence of materials capable of showing nontrivial topological textures of polarization has attracted lots of attention. In particular, structures arising in polar oxide nanostructures due to the delicate interplay between elastic, electrostatic, and gradient energies [1–6], have emerged as an area of great interest. Most studies have been performed on the model system consisting of a superlattice constructed by the periodic repetition of a few layers of a prototype ferroelectric ($PbTiO_3$) and a dielectric ($SrTiO_3$). Various complex patterns of polarization have been theoretically predicted and experimentally observed, depending on the periodicity of the superlattices [7,8], the mechanical boundary conditions [9], and the electric interactions between the polarization charges and residual depolarizing fields. Arrays of polar flux-closure domains [10], vortices [11], skyrmions [12], merons [13], or supercrystals [14] have been reported in some cases coexisting with classical ferroelectric a_1/a_2 domains [15].

In those cases where phases display a rotation of the local dipoles, the minimization of the electrostatic energy cost requires vanishing depolarization charges. This implies that the polarization field has to be divergence-free $\nabla \cdot \mathbf{P} = 0$ with zero net polarization in the sample $\langle \mathbf{P} \rangle = 0$. The latter condition does not necessarily translate into a lack of ordering in the system, in contrast with what happens in the high-temperature paraelectric phase. Indeed, these structures present an underlying coarse grain ordering often associated with the way in which the topological defects arrange in the supercell. These new states of matter come together with exotic functional properties, such as negative capacitance [16–18] or chirality [18–21]. Therefore, the evolution of both the structural and the associated functional properties with external stimuli, such as electric fields, mechanical strain, or thermal fluctuations is

an important question from the applied and the fundamental point of view.

Recent studies have shown the possibility of temperature-induced nonsymmetry breaking Berezinskii-Kosterlitz-Thouless, such as topological phase transitions in low-dimensional ferroelectrics, even when $\langle \mathbf{P} \rangle = 0$, by means of pattern formation or rearrangement of topological defects (polar vortices and antivortices) [22,23]. In these works, the polarization could be regarded as a two-component order parameter where the local dipole moments are *confined to the film plane*. This can occur due to the application of a tensile strain (as in $BaTiO_3$ thin films [22]), or spontaneously (as in crystalline insulator SnTe thin films [23]). As a result, the properties of the celebrated two-dimensional XY model could be recovered in a range of temperatures. Other cases, where the polarization tends to be aligned *perpendicular to the film plane* have also been theoretically explored. In $Pb(Zr_{0.4}Ti_{0.6})O_3$ thin films under compressive strain [24], the system undergoes an inverse phase transition from a highly degenerate labyrinthine phase into a less-symmetric parallel-stripe domain structure upon increasing temperature. Varying the external electric field, the same system undergoes a series of topological phase transitions involving a combination of the elementary topological defects [25]. In particular, in Refs. [24,25], the mechanical boundary conditions force, however, the dipoles to be in a quasi-$\mathbb{Z}_2$ symmetry. In contrast, the vortices in $PbTiO_3/SrTiO_3$ superlattices differ from the previous cases. This has been theoretically predicted from phenomenological theories [26,27], first-principles-based effective Hamiltonian [28], or full first-principles calculations [29], and experimentally demonstrated [11].

Here, the vortices are formed on the (x, z) plane, combining regions (within the center of the domains) where the dipoles are mainly aligned along the z direction with other regions (within the domain wall) where the local polarization rotates and aligns with the x direction (see Fig. 1).
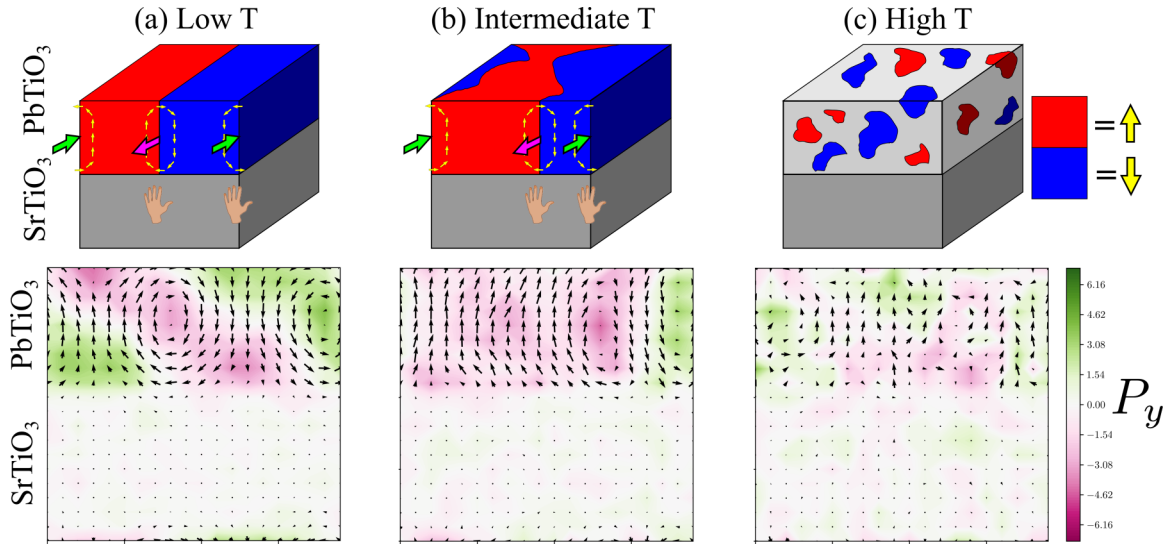
*javier.junquera@unican.es

FIG. 1. Polarization texture in $(PbTiO_3)_{10}/(SrTiO_3)_{10}$ superlattices as a function of temperature: (a) $T = 40$, (b) $T = 80$, and (c) $T = 200$ K. In the top row cartoons, red (blue) regions are the positive (negative) polarization domains along the z direction. Yellow arrows at the domain wall represent the continuous rotation of the polarization within the vortices. Green (magenta) arrows correspond with positive (negative) values of the axial polarization. Left hands indicate the handedness of the structure in the low- and intermediate-temperature regimes. In the bottom row we show the second-principles results for the polarization configuration at the front (x, z) section of the cartoons. The arrows schematize the in-plane components of the polarization whereas the color map represent the axial component along the y direction.

An axial component of the polarization perpendicular to the plane defined by the vortices might coexist with the vorticity, imposing a handedness to each individual vortex [19–21]. Several studies have analyzed the effect on the structure of the periodicity, epitaxial strain, or electric field. However, the effect of temperature on the vortex structure in $PbTiO_3/SrTiO_3$ superlattices has not been explored in much detail.

In this Letter we try to fill this gap, carrying out simulations of $(PbTiO_3)_n/(SrTiO_3)_n$ superlattices of different periodicities with varying temperature using the second-principles methods, as implemented in the SCALE-UP package [30,31]. We find that, at low temperatures, polarization vortices organize in a regular pattern in which clockwise (CW) and counterclockwise (CCW) vortices alternate, leading to a crystal-like structure with well-defined handedness. This chiral crystal melts at a first-order phase transition at a critical temperature of $T_M \approx 73$ K. For $T > T_M$, the vortices become a chiral liquid where long-range order is lost, but the system retains a nonvanishing handedness. Then, a second phase transition occurs at a temperature of $T_C \approx 160$ K where the chiral liquid of polarization vortices loses its handedness. Structural phases and transitions between them are characterized by their corresponding order parameters. In Fig. 1 we show typical snapshots of the local polarization **P** at different temperatures for $(PbTiO_3)_n/(SrTiO_3)_n$ superlattices with $n = 10$. Analogous patterns are obtained for $n = 8$ and $n = 14$ (see the Supplemental Material [32]). Note that the net global polarization is always $\langle \mathbf{P} \rangle = 0$, so no polarization order exists at any temperature. A detailed description of the order parameters, critical temperatures, and the involved broken symmetries will be discussed later on. In the meantime, let us describe the phase phenomenology at a purely qualitative level.

At low temperatures [Fig. 1(a)] we observe a continuously rotating polarization configuration on the (x, z) plane, forming a long-range-ordered array of CW and CCW pairs within the $PbTiO_3$ layer. An axial component of the polarization is clearly detected in our simulations, making the full system chiral [19–21] with a well-defined handedness. This structure is independent of the plane considered along the axial y direction, so the vortex appearance can be described as a perfect crystal of chiral polarization vortex tubes in a three-dimensional framework.

Upon heating, the ordering along the axial direction is lost [Fig. 1(b)]. This occurs above a critical temperature of $T_M \approx 73$ K, upon which the vortex crystal can be considered to melt. Thermal fluctuations induce the movement of the domain walls, a phenomenon that has been associated with the onset of the negative capacitance in these superlattices [16]. Therefore, although the CW and CCW vortex pairs are still clearly visible, one of the domains grows at the expense of the other, although the favoured domain depends on the axial y plane chosen, keeping $\langle \mathbf{P} \rangle = 0$. Interestingly, a modulation of the vortices by a second ordering along their axial direction have been recently reported in $PbTiO_3/SrTiO_3$ superlattices grown on a metallic $SrRuO_3$ substrate [33]. Remarkably, in our system this intermediate temperature phase is also characterized by the maintenance of the chiral behavior, so it can be described as a chiral liquid of polarization vortices. Temperature-induced domain melting in these superlattices has also been reported in the context of negative capacitance [16].

Finally, there exists a high temperature phase [Fig. 1(c)], again above some critical temperature $T_C \approx 160$ K where a disordered paraelectric phase is found. In this regime, thermal fluctuations are strong enough to break chiral symmetry of the
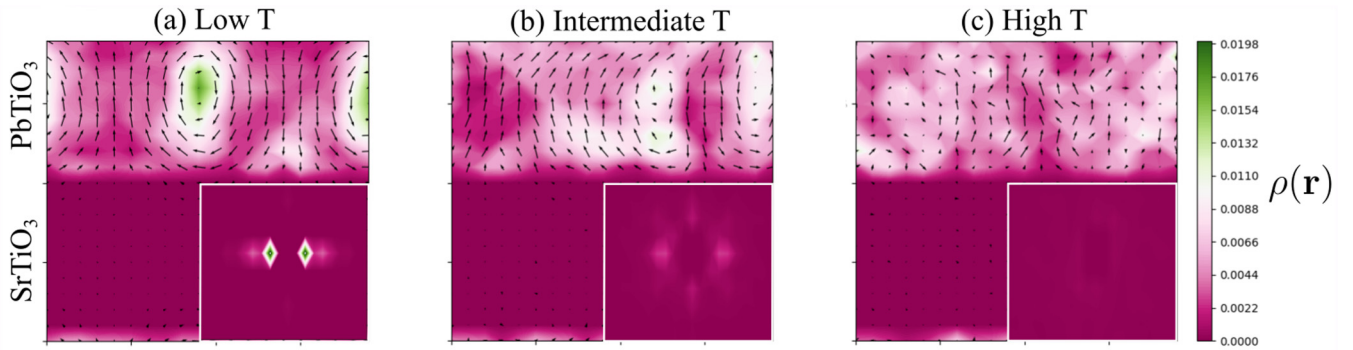
FIG. 2. Curl density for the different temperature regimes. Black arrows indicate the local dipoles, projected onto the (x, z) plane. (a) Chiral-crystalline-ordered phase at $T = 40$ K. (b) Chiral-liquid phase at $T = 80$ K. (c) High-temperature disordered phase at $T = 200$ K. The insets represent the Fourier transform $[\widehat{\rho}(\mathbf{q})]$ of the curl density diagrams. The zero-mode component of the Fourier component is not represented in the insets to avoid saturation.

vortex liquid and polarization orientations become randomly distributed.

a. Order parameter for the crystal to liquid phase transition. In the low-temperature phase the polarization vector field aligns within the domains along the y and z directions, whereas it rotates around specific lattice positions where CW (or CCW) vortices appear. The simplest way to define a vortex position is to compute the curl field, $|\nabla \times \mathbf{P}(\mathbf{r})|$ where $\nabla \equiv (\partial_x, \partial_y, \partial_z)$, $\mathbf{r} = (r_x, r_y, r_z)$ is the position in the supercell, and the absolute value is taken to include both CW and CCW vortices. Note that this curl field will take finite values at the lattice sites around which the vortices are located, whereas it will vanish in regions where the polarization vector is aligned. The density of vortices can then be calculated as

$$\rho(\mathbf{r}) = \frac{|\nabla \times \mathbf{P}(\mathbf{r})|}{\iint dx\, dz\, |\nabla \times \mathbf{P}(\mathbf{r})|}. \qquad (1)$$

By construction, $\rho(\mathbf{r})$ is normalized for every (x, z) plane containing vortex pairs. As in standard fluids, from this density a regular arrangement and a random spatial distribution of vortices can be distinguished by computing the structure factor, $S(\mathbf{q}) = \langle \widehat{\rho}_y(\mathbf{q}) \widehat{\rho}_y(-\mathbf{q}) \rangle$, where $\widehat{\rho}_y(\mathbf{q}) = \iint dx\, dz\, \rho(\mathbf{r}) e^{-i\mathbf{q} \cdot \mathbf{r}_\perp}$, $\mathbf{q} = (q_x, q_z)$ is the wave-number vector, and $\mathbf{r}_\perp$ corresponds to the component of the position on a given y plane. Brakets $\langle \cdots \rangle$ stand for an average over both all the axial y planes in the supercell and snapshots of the Monte Carlo simulations at each temperature. A regular lattice of vortices (i.e., a crystal phase) corresponds to $S(\mathbf{q})$ showing a peak at some $\mathbf{q}_m$, reflecting the regular distribution of the density $\rho(\mathbf{r})$. In contrast, for the case of an unstructured random distribution of vortices (i.e., a liquid phase) all Fourier components of the density become negligible except for the zero-mode $\mathbf{q} = 0$ where the structure factor amplitude concentrates. The curl density is shown in Fig. 2 together with its Fourier transform (see the insets). Prominent peaks with fixed periodicity (coming from the periodic arrangement of CW and CCW vortex cores) appear in the low-temperature phase. As temperature increases above T_M, the curl density spreads, although it still peaks at the location of the vortices. However, the relative position between vortex cores and the distance between them varies depending on the axial section analyzed. Finally, the

curl density is more homogeneous over the (x, z) section plane at the high-temperature phase above T_C. By analogy with liquid-solid phase transitions in standard fluids [34], we define the order parameter,

$$\Psi(T) = \frac{S(\mathbf{q}_m)}{\rho_0^2}, \qquad (2)$$

as a function of temperature [32]. Note that $\Psi(T)$ takes finite values whereas the system is in the crystal phase and vanishes in the disordered vortex liquid phase.

b. Order parameter for the chiral to achiral phase transition. The order parameter that best captures the breakdown of chiral symmetry is the helicity $\mathcal{H}$ of the chiral field. In our case, the chiral field is the polarization, and for the helicity we borrow the definition from fluid dynamics as [35]

$$\mathcal{H} = \int d^3\mathbf{r}\, \mathbf{P}(\mathbf{r}) \cdot [\nabla \times \mathbf{P}(\mathbf{r})], \qquad (3)$$

where now the integral is over the whole volume, instead of (x, z) planes. Note that $\mathcal{H}$ changes sign upon a mirror symmetry reflection [36]. A nonzero helicity means chirality or lack of mirror symmetry of the polarization texture: right (left) handedness can be associated with positive (negative) values of $\mathcal{H}$. Accordingly, the helicity modulus $|\mathcal{H}|$ quantifies the strength of the chirality symmetry breaking (see Fig. 3). The dependence with temperature of the spatial organization Eq. (2) and helicity Eq. (3) order parameters for different periodicity of the superlattice is summarized in Fig. 4. At low temperatures, after equilibrium is reached, the vortices self-organize in a crystalline chiral phase [Fig. 1(a)]. The spatial organization order parameter $\Psi(T)$ reduces as temperature increases and, at a critical temperature $T_M \approx 73$ K, the system suffers a first-order melting phase transition, where Ψ abruptly drops to zero, whereas the helicity order parameter remains finite [Figs. 3(a) and 3(b)], so the liquid of vortices remains chiral for a wide range of temperatures. This liquid chiral phase is stable, although with reduced values of the helicity modulus, up to the critical temperature of $T_C \approx 160$ K where a second-order phase transition occurs. Above T_C thermal fluctuations are strong enough to destroy chiral ordering, leading to an achiral phase with a vanishing value of the helicity. These phase transitions are
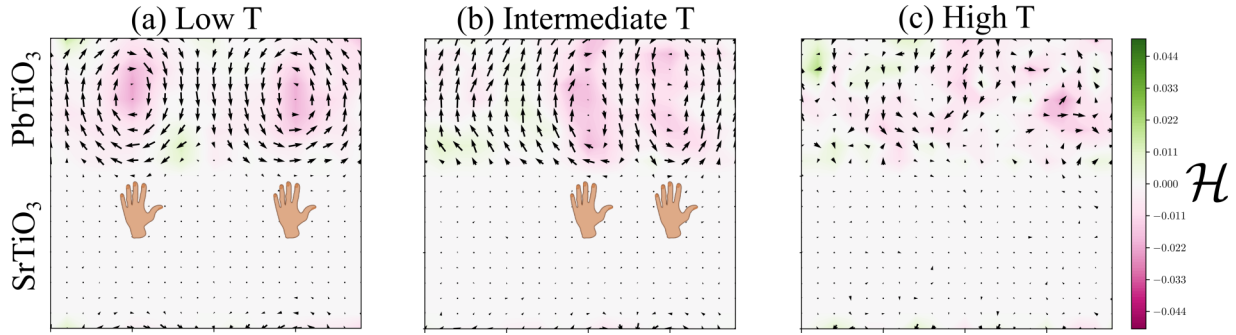
FIG. 3. Normalized helicity at temperatures of (a) $T = 40$, (b) $T = 80$, and (c) $T = 200$ K. Left hands indicate the handedness of the structure in the low- and intermediate- temperature regimes. The absence of hands in the high-temperature regime stands for its achiral character. The color map represents the system-size independent normalized helicity [32].

independent of the periodicity of the system in the computed range $8 < n < 14$. To summarize we present second-principles simulations of $(PbTiO_3)_n/(SrTiO_3)_n$ superlattices and show that, despite the net polarization remains zero for all temperatures, the system exhibits symmetry-breaking phase transitions (from crystalline-chiral, melting into a liquid chiral, and finally to liquid achiral) as temperature is varied.

The presented results might have important consequences in other functional properties of the superlattices. In particular, the dielectric properties might depart from the classical Curie-Weiss behavior as a function of temperature expected for traditional ferroelectric to paraelectric phase transitions. It is worth remarking here that the term *liquid* phase in this context essentially means a phase with translational invariance as opposed to the low-temperature crystalline phase where this symmetry is broken. Indeed, the liquid phase we observe shows some glassy features. We expect that the structural phases we report here for $PbTiO_3/SrTiO_3$ superlattices are quite generic and might be found in other similar systems. For

instance, using similar structural factors as the one employed here the melting of a two-dimensional magnetic skyrmion lattice has been recently reported [37]. Vortex lattice melting has also been reported in high-temperature superconductors [38]. However, these phases may be difficult to find experimentally, or even numerically due to the existence of long-lived metastable states. In particular, the melting point that separates the vortex crystal and liquid phases is a first-order critical point and as occurs in conventional fluids, it shows hysteresis phenomena. In fact, in our simulations (not shown) we checked that, starting in the chiral liquid phase ($T > T_M$) and lowering the temperature, the system may remain in the liquid phase for extremely long times, even for temperatures quite below T_M. This is analogous to the supercooled liquids that can be found below the freezing point in conventional fluids. Indeed, in our simulations we find that below T_M an external perturbation as, for instance, a change in the applied strain, can be enough to drive a rapid crystalization of the metastable vortex liquid phase, similarly as occurs in conventional fluids. We remark that all our simulations were performed at zero applied strain. This might be a tuning parameter that affects the structural phases. It would be extremely interesting to study how the phases we report here depend on the applied strain, specially in the strong expansive limit when the polarization field is progressively forced to lay on the (x, y) plane and might become effectively two dimensional.
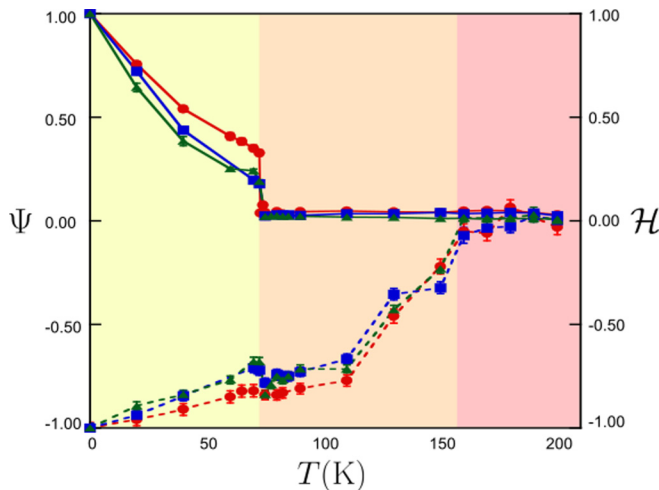

FIG. 4. Structural order parameter Ψ [Eq. (2)] and the helicity $\mathcal{H}$ [Eq. (3)] as a function of temperature for different periodicities of the superlattice: $n = 8$ (red circles), $n = 10$ (blue squares), and $n = 14$ (green triangles). Solid (dashed) lines interpolate the different values of Ψ ($\mathcal{H}$) at different temperatures. Error bars are associated with the fluctuations of the order parameter defined by its variance.

[1] J. M. Gregg, Exotic domain states in ferroelectrics: Searching for vortices and skyrmions, Ferroelectrics **433**, 74 (2012).

[2] J. Seidel, R. K. Vasudevan, and N. Valanoor, Topological structures in multiferroics domain walls, skyrmions and vortices, Adv. Electron. Mater. **2**, 1500292 (2016).

[3] J. Hlinka and P. Ondrejkovic, Chapter four - skyrmions in ferroelectric materials, in *Recent Advances in Topological Ferroics and their Dynamics*, Solid State Physics, Vol. 70, edited by R. L. Stamps and H. Schultheiß (Academic Press, San Diego, 2019), pp. 143–169.

[4] G. F. Nataf, M. Guennou, J. M. Gregg, D. Meier, J. Hlinka, E. K. H. Salje, and J. Kreisel, Domain-wall engineering and topological defects in ferroelectric and ferroelastic materials, Nat. Rev. Phys. **2**, 634 (2020).

[5] S. Chen, S. Yuan, Z. Hou, Y. Tang, J. Zhang, T. Wang, K. Li, W. Zhao, X. Liu, L. Chen, L. W. Martin, and Z. Chen, Recent progress on topological structures in ferroic thin films and heterostructures, Adv. Mater. **33**, 2000857 (2021).

[6] Y. L. Tang, Y. L. Zhu, and X. L. Ma, Topological polar structures in ferroelectric oxide films, J. Appl. Phys. **129**, 200904 (2021).

[7] Z. Hong, A. R. Damodaran, F. Xue, S. L. Hsu, J. Britson, A. K. Yadav, C. T. Nelson, J. J. Wang, J. F. Scott, L. W. Martin, R. Ramesh, and L. Q. Chen, Stability of polar vortex lattice in ferroelectric superlattices, Nano Lett. **17**, 2246 (2017).

[8] P. Zubko, N. Jecklin, A. Torres-Pardo, P. Aguado-Puente, A. Gloter, C. Lichtensteiger, J. Junquera, O. Stéphan, and J.-M. Triscone, Electrostatic coupling and local structural distortions at interfaces in ferroelectric/paraelectric superlattices, Nano Lett. **12**, 2846 (2012).

[9] S. Li, Y. Wang, Y. Zhu, Y. Tang, Y. Liu, J. Ma, M. Han, B. Wu, and X. Ma, Evolution of flux-closure domain arrays in oxide multilayers with misfit strain, Acta Mater. **171**, 176 (2019).

[10] Y. L. Tang, Y. L. Zhu, X. L. Ma, A. Y. Borisevich, A. N. Morozovska, E. A. Eliseev, W. Y. Wang, Y. J. Wang, Y. B. Xu, Z. D. Zhang, and S. J. Pennycook, Observation of a periodic array of flux-closure quadrants in strained ferroelectric PbTiO$_3$ films, Science **348**, 547 (2015).

[11] A. K. Yadav, C. T. Nelson, S. L. Hsu, Z. Hong, J. D. Clarkson, C. M. Schlepütz, A. R. Damodaran, P. Shafer, E. Arenholz, L. R. Dedon, D. Chen, A. Vishwanath, A. M. Minor, L. Q. Chen, J. F. Scott, L. W. Martin, and R. Ramesh, Observation of polar vortices in oxide superlattices, Nature (London) **530**, 198 (2016).

[12] S. Das, Y. L. Tang, Z. Hong, M. A. P. Gonçalves, M. R. McCarter, C. Klewe, K. X. Nguyen, F. Gómez-Ortiz, P. Shafer, E. Arenholz, V. A. Stoica, S.-L. Hsu, B. Wang, C. Ophus, J. F. Liu, C. T. Nelson, S. Saremi, B. Prasad, A. B. Mei, D. G. Schlom *et al.*, Observation of room-temperature polar skyrmions, Nature (London) **568**, 368 (2019).

[13] Y. J. Wang, Y. P. Feng, Y. L. Zhu, Y. L. Tang, L. X. Yang, M. J. Zou, W. R. Geng, M. J. Han, X. W. Guo, B. Wu, and X. L. Ma, Polar meron lattice in strained oxide ferroelectrics, Nature Mater. **19**, 881 (2020).

[14] V. A. Stoica, N. Laanait, C. Dai, Z. Hong, Y. Yuan, Z. Zhang, S. Lei, M. R. McCarter, A. Yadav, A. R. Damodaran, S. Das, G. A. Stone, J. Karapetrova, D. A. Walko, X. Zhang, L. W. Martin, R. Ramesh, L.-Q. Chen, H. Wen, V. Gopalan *et al.*, Optical creation of a supercrystal with three-dimensional nanoscale periodicity, Nature Mater. **18**, 377 (2019).

[15] A. R. Damodaran, J. D. Clarkson, Z. Hong, H. Liu, A. K. Yadav, C. T. Nelson, S.-L. Hsu, M. R. McCarter, K.-D. Park, V. Kravtsov, A. Farhan, Y. Dong, Z. Cai, H. Zhou, P. Aguado-Puente, P. García-Fernández, J. Íñiguez, J. Junquera, A. Scholl, M. B. Raschke *et al.*, Phase coexistence and electric-field control of toroidal order in oxide superlattices, Nature Mater. **16**, 1003 (2017).

[16] P. Zubko, J. C. Wojdeł, M. Hadjimichael, S. Fernandez-Pena, A. Sené, I. Luk'yanchuk, J.-M. Triscone, and J. Íñiguez, Negative capacitance in multidomain ferroelectric superlattices, Nature (London) **534**, 524 (2016).

[17] A. K. Yadav, K. X. Nguyen, Z. Hong, P. García-Fernández, P. Aguado-Puente, C. T. Nelson, S. Das, B. Prasad, D. Kwon, S. Cheema, A. I. Khan, C. Hu, J. Íñiguez, J. Junquera, L.-Q. Chen, D. A. Muller, R. Ramesh, and S. Salahuddin, Spatially resolved steady-state negative capacitance, Nature (London) **565**, 468 (2019).

[18] S. Das, Z. Hong, V. A. Stoica, M. A. P. Gonçalves, Y. T. Shao, E. Parsonnet, E. J. Marksz, S. Saremi, M. R. McCarter, A. Reynoso, C. J. Long, A. M. Hagerstrom, D. Meyers, V. Ravi, B. Prasad, H. Zhou, Z. Zhang, H. Wen, F. Gómez-Ortiz, P. García-Fernández *et al.*, Local negative permittivity and topological phase transition in polar skyrmions, Nature Mater. **20**, 194 (2021).

[19] L. Louis, I. Kornev, G. Geneste, B. Dkhil, and L. Bellaiche, Novel complex phenomena in ferroelectric nanocomposites, J. Phys.: Condens. Matter **24**, 402201 (2012).

[20] P. Shafer, P. García-Fernández, P. Aguado-Puente, A. R. Damodaran, A. K. Yadav, C. T. Nelson, S.-L. Hsu, J. C. Wojdeł, J. Íñiguez, L. W. Martin, E. Arenholz, J. Junquera, and R. Ramesh, Emergent chirality in the electric polarization texture of titanate superlattices, Proc. Natl. Acad. Sci. USA **115**, 915 (2018).

[21] P. Behera, M. A. May, F. Gómez-Ortiz, S. Susarla, S. Das, C. T. Nelson, L. Caretta, S.-L. Hsu, M. R. McCarter, B. H. Savitzky, E. S. Barnard, A. Raja, Z. Hong, P. García-Fernandez, S. W. Lovesey, G. van der Laan, P. Ercius, C. Ophus, L. W. Martin, J. Junquera *et al.*, Electric field control of chirality, Sci. Adv. **8**, eabj8030 (2022).

[22] Y. Nahas, S. Prokhorenko, I. Kornev, and L. Bellaiche, Emergent Berezinskii-Kosterlitz-Thouless Phase in Low-Dimensional Ferroelectrics, Phys. Rev. Lett. **119**, 117601 (2017).

[23] C. Xu, Y. Nahas, S. Prokhorenko, H. Xiang, and L. Bellaiche, Berezinskii-Kosterlitz-Thouless phase in two-dimensional ferroelectrics, Phys. Rev. B **101**, 241402(R) (2020).

[24] Y. Nahas, S. Prokhorenko, J. Fischer, B. Xu, C. Carrétéro, S. Prosandeev, M. Bibes, S. Fusil, B. Dkhil, V. Garcia, and L. Bellaiche, Inverse transition of labyrinthine domain patterns in ferroelectric thin films, Nature (London) **577**, 47 (2020).

[25] Y. Nahas, S. Prokhorenko, Q. Zhang, V. Govinden, N. Valanoor, and L. Bellaiche, Topology and control of self-assembled domain patterns in low-dimensional ferroelectrics, Nat. Commun. **11**, 5779 (2020).

[26] G. B. Stephenson and K. R. Elder, Theory for equilibrium 180° stripe domains in pbtio3 films, J. Appl. Phys. **100**, 051601 (2006).

[27] A. M. Bratkovsky and A. P. Levanyuk, Continuous theory of ferroelectric states in ultrathin films with real electrodes, J. Comput. Theor. Nanosci. **6**, 465 (2009).

[28] I. Kornev, H. Fu, and L. Bellaiche, Ultrathin Films of Ferroelectric Solid Solutions under a Residual Depolarizing Field, Phys. Rev. Lett. **93**, 196104 (2004).

[29] P. Aguado-Puente and J. Junquera, Structural and energetic properties of domains in $PbTiO_3/SrTiO_3$ superlattices from first principles, Phys. Rev. B **85**, 184105 (2012).

[30] J. C. Wojdeł, P. Hermet, M. Ljunberg, P. Ghosez, and J. Íñiguez, First-principles model potentials for lattice-dynamical studies: general methodology and example of application to ferroic perovskite oxides, J. Phys.: Condens. Matter **25**, 305401 (2013).

[31] P. García-Fernández, J. C. Wojdeł, J. Íñiguez, and J. Junquera, Second-principles method for materials simulations including electron and lattice degrees of freedom, Phys. Rev. B **93**, 195137 (2016).

[32] See Supplemental Material at http://link.aps.org/supplemental/10.1103/PhysRevB.105.L220103 which includes: the description of the methods, figures of the dipole patterns as a function of temperature for periodicities of $n = 8$ and $n = 14$, derivation of the structural order parameter, and a discussion on the normalization of the helicity.

[33] D. Rusu, J. J. P. Peters, T. P. A. Hase, J. A. Gott, G. A. A. Nisbet, J. Strempfer, D. Haskel, S. D. Seddon, R. Beanland, A. M. Sanchez, and M. Alexe, Ferroelectric incommensurate spin crystals, Nature (London) **602**, 240 (2022).

[34] P. M. Chaikin and T. C. Lubensky, *Principles of Condensed Matter Physics* (Cambridge University Press, Cambridge, UK, 1995).

[35] H. Moffatt and R. Ricca, Helicity and the Clugreanu invariant, Proc. R. Soc. London, Ser. A **439**, 411 (1992).

[36] H. K. Moffatt, Helicity and singular structures in fluid dynamics, Proc. Natl. Acad. Sci. USA **111**, 3663 (2014).

[37] P. Huang, T. Schönenberger, M. Cantoni, L. Heinen, A. Magrez, A. Rosch, F. Carbone, and H. M. Rønnow, Melting of a skyrmion lattice to a skyrmion liquid via a hexatic phase, Nat. Nanotechnol. **15**, 761 (2020).

[38] G. Blatter, M. V. Feigel'man, V. B. Geshkenbein, A. I. Larkin, and V. M. Vinokur, Vortices in high-temperature superconductors, Rev. Mod. Phys. **66**, 1125 (1994).